PHYSICAL REVIEW D **88,** 114022 (2013)

KK MC 4.22: Coherent exclusive exponentiation of electroweak corrections for $f\bar{f} \to f'\bar{f}'$ at the LHC and muon colliders

S. Jadach,[1,2] B. F. L. Ward,[1] and Z. Wąs[2]

[1]*Baylor University, Waco, Texas 76798-7316, USA*

[2]*Institute of Nuclear Physics, Polish Academy of Sciences, ul. Radzikowskiego 152, 31-342 Cracow, Poland*

(Received 15 July 2013; published 6 December 2013)

We present the upgrade of the coherent exclusive exponentiation realization of the Yennie-Frautschi-Suura theory used in our Monte Carlo ($\mathcal{KK}$ MC) to the processes $f\bar{f} \to f'\bar{f}'$, $f = \mu, \tau, q, \nu_\ell$, $f' = e, \mu, \tau, q, \nu_\ell$, $q = u, d, s, c, b, t$, $\ell = e, \mu, \tau$ with $f \neq f'$, with an eye toward the precision physics of the LHC and possible high energy muon colliders. We give a brief summary of the coherent exclusive exponentiation theory in comparison to the older exclusive exponentiation theory and illustrate theoretical results relevant to the LHC and possible muon collider physics programs.

DOI: 10.1103/PhysRevD.88.114022 PACS numbers: 12.15.−y, 12.15.Lk, 13.40.Ks

I. INTRODUCTION

Given that the era of precision QCD at the LHC is upon us, by which we mean theoretical precision tags at or below 1% in QCD corrections to LHC physical processes, computation of higher order electroweak (EW) corrections are also required: in the single Z production process at the LHC for example, a u quark anti-u quark annihilation hard process at the Z pole has a radiation probability strength factor of $\frac{4}{9}\frac{2\alpha}{\pi}(\ln(M_Z^2/m_u^2) - 1) \cong 0.038$ if we use the value $m_u \cong 5.0$ MeV, the current quark mass value—we return to the best choice for the quark masses below. Evidently, we have to take these EW effects into account at the per mille level if we do not wish that they spoil the sub-1% precision QCD we seek in LHC precision QCD studies [1]. Indeed, when the cut on the respective energy of the emitted photons is at $v_{\min}$ in units of the reduced cms effective beam energy, the 0.038 strength factor above is enhanced to $0.038 \ln(1/v_{\min})$ and can easily become $\mathcal{O}(1)$. This means we have to use resummation, realized by MC event generator methods, of the type we have pioneered in Refs. [2] to make contact with observation based on arbitrary cuts in any precise way. We call the reader's attention here to the approaches of Refs. [3–7] to EW corrections to such heavy gauge boson production at the LHC. It is well known from large electron positron (LEP) collider studies [8] that using only the exact $\mathcal{O}(\alpha)$ EW corrections is inadequate for per mille level accuracy on these corrections. Our studies below will show that this is still the case. This means that the approaches in Refs. [3,5–7] must be extended to higher orders for precision LHC studies. We comment further below on the relation of our approach to that in Ref. [4] as well.[1]

Presently, we recall that in the case of single $Z/\gamma*$ production in high energy e^+e^- annihilation our state of the art realization of such resummation is the coherent exclusive (CEEX) Yennie-Frautschi-Suura (YFS) [11,12] exponentiation we have realized by MC methods in the $\mathcal{KK}$ MC[2] in Ref. [13]. We conclude that we therefore need to extend the incoming states that the $\mathcal{KK}$ MC allows to include the incoming quarks and antiquarks in the protons colliding at the LHC. Previous versions of $\mathcal{KK}$ MC even though not adapted for the LHC were already found useful in estimations of theoretical systematic errors of other calculations [14,15]. We denote the new version of $\mathcal{KK}$ MC by version number 4.22, $\mathcal{KK}$ MC 4.22. Our aims in the current discussion in its regard are to summarize briefly on the main features of YFS/CEEX exponentiation [12,16] in the standard model (SM) EW theory, as this newer realization of the YFS theory is not a generally familiar one, to discuss the changes required to extend the incoming beam choices in the $\mathcal{KK}$ MC from the original e^+e^- incoming state in Ref. [13] to the more inclusive choices $f\bar{f}$, $f = e, \mu, \tau, q, \nu_\ell$, $q = u, d, s, b$, $\ell = e, \mu, \tau$, and to present examples of theoretical results relevant for the LHC and possible muon collider [17] precision physics programs. For example, the muon collider physics program involves precision studies of the properties of the recently discovered Brout-Englert-Higgs boson [18] candidate [19,20] and treatment of the effects of higher order EW

[1]We remind the reader that, as it is done in Ref. [4] for example, in the hadron collider environment, one can also use DGLAP-CS [9,10] theory for the large QED corrections in the ISR, so that standard factorization methods are used to remove the big QED logs from the reduced hard cross sections and they occur in the solution of the QED evolution equations for the parton distribution functions (PDF's) which can be solved from the quark mass m_q to the factorization scale $Q \simeq M_Z$ here because QED is an infrared free theory; in what follows, we argue that we improve on the treatment of such effects with resummation methods we discuss presently.

[2]The name $\mathcal{KK}$ MC derives from the fact that the program was published in the last year of the second millenium, where we note that K is the first letter of the Greek word Kilo, and from the fact that two of us (S. J. and Z. W.) were located in Krakow, Poland and the other of us (B. F. L. W.) was located in Knoxville, TN, USA at the inception of the code.

corrections will be essential to the success of the program, as we illustrate below.

In the next section, we review the older EEX exclusive realization and summarize the newer CEEX exclusive realization of the YFS [11] resummation in the SM EW theory; for, the YFS resummation is not generally familiar so that our review of the material in Refs. [2,12,16] will aid the unfamiliar reader to follow the current discussion. We do this in the context of e^+e^- annihilation physics programs for definiteness for historical reasons. In this way we illustrate the latter's advantages over the former, which is also very successful. We also stress the key common aspects of our MC implementations of the two approaches to exponentiation, such as the exact treatment of phase space in both cases, the strict realization of the factorization theorem, etc. We stress that both of the realizations of YFS exponentiation are available in the $\mathcal{KK}$ MC 4.22 where both allow for the new incoming beams choices. This gives us important cross-check avenues required to establish the final precision tag of our results. In Sec. III, we discuss and illustrate the extension of the choices of the incoming beams in the $\mathcal{KK}$ MC realization of CEEX/EEX. We illustrate results which quantify the size of the EW higher order corrections in LHC and muon collider physics scenarios. Specific realizations of the results we present here in the context of a parton shower environment will appear elsewhere [21]. Sec. IV contains our summary. Appendix A contains a sample output.

II. REVIEW OF STANDARD MODEL CALCULATIONS FOR e^+e^- ANNIHILATION WITH YFS EXPONENTIATION

There are many examples of successful applications [2] of our approach to the MC realization of the YFS theory of exponentiation for e^+e^- annihilation physics: (i), for $e^+e^- \to f\bar{f} + n\gamma$, $f = \tau, \mu, d, u, s, c$ there are YFS1 (1987-1989) $\mathcal{O}(\alpha^1)_{\rm exp}$ ISR, YFS2 $\in$ KORALZ (1989-1990), $\mathcal{O}(\alpha^1 + h.o.LL)_{\rm exp}$ ISR, YFS3 $\in$ KORALZ (1990-1998), $\mathcal{O}(\alpha^1 + h.o.LL)_{\rm exp}$ ISR + FSR, and $\mathcal{KK}$ MC (98-02) $\mathcal{O}(\alpha^2 + h.o.LL)_{\rm exp}$ ISR + FSR + IFI with $d\sigma/\sigma = 0.2\%$; (ii), for $e^+e^- \to e^+e^- + n\gamma$ for $\theta < 6^\circ$ there are BHLUMI 1.x, (1987-1990), $\mathcal{O}(\alpha^1)_{\rm exp}$ and BHLUMI 2.x,4.x, (1990-1996), $\mathcal{O}(\alpha^1 + h.o.LL)_{\rm exp}$ with $d\sigma/\sigma = 0.061\%$; (iii), for $e^+e^- \to e^+e^- + n\gamma$ for $\theta > 6^\circ$ there is BHWIDE (1994-1998), $\mathcal{O}(\alpha^1 + h.o.LL)_{\rm exp}$ with $d\sigma/\sigma = 0.2(0.5)\%$ at the Z peak (just off the Z peak); (iv), for $e^+e^- \to W^+W^- + n\gamma$, $W^\pm \to f\bar{f}$ there is KORALW (1994-2001); and, (v), for $e^+e^- \to W^+W^- + n\gamma$, $W^\pm \to f\bar{f}$ there is YFSWW3 (1995-2001), YFS exponentiation + Leading Pole Approximation with $d\sigma/\sigma = 0.4\%$ at LEP2 energies above the WW threshold. The typical MC realization we effect in Refs. [2] is in the form of the "matrix element $\times$ exact phase space" principle, as we illustrate in the following diagram:

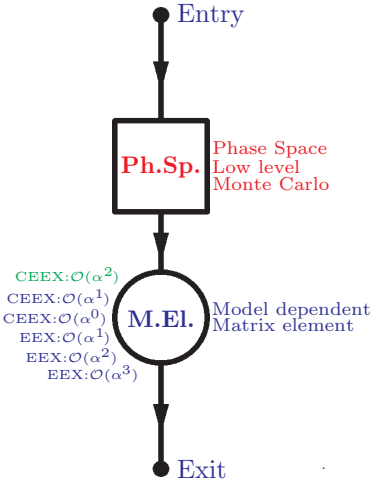

In practice it means the following:

(i) The universal exact phase-space MC simulator is a separate module producing "raw events" (with importance sampling).

(ii) The library of several types of SM/QED matrix elements which provides the "model weight" is another independent module (the $\mathcal{KK}$MC example is shown).

(iii) Tau decays and hadronization come afterwards of course.

The main steps in YFS exponentiation are the reorganization of the perturbative complete $\mathcal{O}(\alpha^\infty)$ series such that IR-finite $\bar{\beta}$ components are isolated (factorization theorem) and the truncation of the IR-finite $\bar{\beta}$s to finite $\mathcal{O}(\alpha^n)$ with the attendant calculation of them from Feynman diagrams recursively. We illustrate here the respective factorization for overlapping IR divergences for the 2γ case $-R_{12} \in R_1$ and $R_{12} \in R_2$ as they are shown in the following picture:

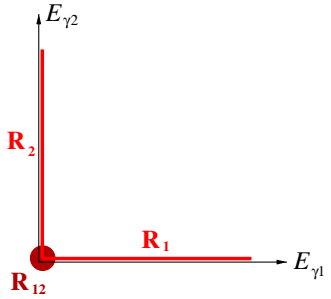

$$D_0(p_{f_1}, p_{f_2}, p_{f_3}, p_{f_4}) = \bar{\beta}_0(p_{f_1}, p_{f_2}, p_{f_3}, p_{f_4});$$

$$p_{f_1} + p_{f_2} = p_{f_3} + p_{f_4}$$
$$D_1(p_f; k_1) = \bar{\beta}_0(p_f)\tilde{S}(k_1) + \bar{\beta}_1(p_f; k_1);$$

$$p_{f_1} + p_{f_2} \neq p_{f_3} + p_{f_4}$$
$$D_2(k_1, k_2) = \bar{\beta}_0\tilde{S}(k_1)\tilde{S}(k_2) + \bar{\beta}_1(k_1)\tilde{S}(k_2) + \bar{\beta}_1(k_2)\tilde{S}(k_1) + \bar{\beta}_2(k_1, k_2).$$

Note: $\bar{\beta}_0$ and $\bar{\beta}_1$ are used beyond their usual (Born and 1γ) respective phase spaces. A kind of smooth "extrapolation"

or "projection" is always necessary. We see that a recursive order-by-order calculation of the IR-finite $\bar{\beta}$s to a given fixed $\mathcal{O}(\alpha^n)$ is possible: specifically,

$$\bar{\beta}_0(p_{f_1}, p_{f_2}, p_{f_3}, p_{f_4}) = D_0(p_{f_1}, p_{f_2}, p_{f_3}, p_{f_4}),$$

$$\bar{\beta}_1(p_f; k_1) = D_1(p_f; k_1) - \bar{\beta}_0(p_f)\tilde{S}(k_1),$$

$$\bar{\beta}_2(k_1, k_2) = D_2(k_1, k_2) - \bar{\beta}_0\tilde{S}(k_1)\tilde{S}(k_2) - \bar{\beta}_1(k_1)\tilde{S}(k_2) - \bar{\beta}_1(k_2)\tilde{S}(k_1), \ldots,$$

In the classic EEX/YFS schematically the β's are truncated to $\mathcal{O}(\alpha^1)$, in the ISR example. For $e^-(p_1, \lambda_1) + e^+(p_2, \lambda_2) \to f(q_1, \lambda_1') + \bar{f}(q_2, \lambda_2') + \gamma(k_1, \sigma_1) + \cdots + \gamma(k_n, \sigma_n)$, we have

$$\sigma = \sum_{n=0}^{\infty} \int_{m_\gamma} d\Phi_{n+2} e^{Y(m_\gamma)} D_n(q_1, q_2, k_1, \ldots, k_n) \quad (1)$$

with

$$D_0 = \bar{\beta}_0, \quad D_1(k_1) = \bar{\beta}_0\tilde{S}(k_1) + \bar{\beta}_1(k_1),$$
$$D_2(k_1, k_2) = \bar{\beta}_0\tilde{S}(k_1)\tilde{S}(k_2) + \bar{\beta}_1(k_1)\tilde{S}(k_2) + \bar{\beta}_1(k_2)\tilde{S}(k_1),$$
$$\begin{aligned} D_n(k_1, k_2 \ldots k_n) = {} & \bar{\beta}_0\tilde{S}(k_1)\tilde{S}(k_2)\ldots\tilde{S}(k_n) \\ & + \bar{\beta}_1(k_1)\tilde{S}(k_2)\tilde{S}(k_3)\ldots\tilde{S}(k_n) \\ & + \tilde{S}(k_1)\bar{\beta}_1(k_2)\tilde{S}(k_3)\ldots\tilde{S}(k_n) + \cdots \\ & + \tilde{S}(k_1)\tilde{S}(k_2)\tilde{S}(k_3)\ldots\bar{\beta}_1(k_n). \end{aligned} \quad (2)$$

The real soft factors and the IR-finite building blocks are

$$\begin{aligned} \tilde{S}(k) &= \sum_\sigma |\mathbb{S}_\sigma(k)|^2 = |\mathbb{S}_+(k)|^2 + |\mathbb{S}_-(k)|^2 \\ &= -\frac{\alpha}{4\pi^2}\left(\frac{q_1}{kq_1} - \frac{q_2}{kq_2}\right)^2 \\ \bar{\beta}_0 &= (e^{-2\alpha\Re B_4}\sum_\lambda |\mathcal{M}_\lambda^{\text{Born+Virt}}|^2)|_{\mathcal{O}(\alpha^1)}, \\ \bar{\beta}_1(k) &= \sum_{\lambda\sigma} |\mathcal{M}_{\lambda\sigma}^{1\text{-PHOT}}|^2 - \sum_\sigma |\mathbb{S}_\sigma(k)|^2 \sum_\lambda |\mathcal{M}_\lambda^{\text{BORN}}|^2, \end{aligned} \quad (3)$$

with λ = fermion helicity, σ = photon helicity, and everything being in terms of $\sum_{\text{spin}} |\cdots|^2$.

The newer CEEX replaces older the EEX, where both are derived from the YFS theory [11]: EEX, Exclusive EXponentiation, is very close to the original Yennie-Frautschi-Suura formulation, which is also now featured in the MC's Herwig++ [22] and Sherpa [23] for particle decays. We need to stress that CEEX, Coherent EXclusive exponentiation, is an extension of the YFS theory. Because of its coherence CEEX is friendly to quantum coherence among the Feynman diagrams, so that we have the complete $|\sum_{\text{diagr}}^n \mathcal{M}_i|^2$ rather than the often incomplete $\sum_{i,j}^{n^2} \mathcal{M}_i \mathcal{M}_j^*$. It follows that we get readily the proper treatment of narrow resonances, $\gamma \oplus Z$ exchanges, $t \oplus s$ channels, ISR $\oplus$ FSR, angular ordering, etc. KORALZ/YFS2, BHLUMI, BHWIDE, YFSWW, KoralW and KORALZ are examples of the EEX formulation in our MC event generator approach; $\mathcal{KK}$MC is the only example of the CEEX formulation.

Using the example of ISR $\mathcal{O}(\alpha^1)$ we illustrate CEEX schematically for the process $e^-(p_1, \lambda_1) + e^+(p_2, \lambda_2) \to f(q_1, \lambda_1') + \bar{f}(q_2, \lambda_2') + \gamma(k_1, \sigma_1) + \cdots + \gamma(k_n, \sigma_n)$. We have

$$\begin{aligned} \sigma = \sum_{n=0}^{\infty} \int_{m_\gamma} d\Phi_{n+2} \sum_{\lambda, \sigma_1, \ldots, \sigma_n} & |e^{\alpha B(m_\gamma)} \\ & \times \mathcal{M}_{n,\sigma_1,\ldots,\sigma_n}^{\lambda}(k_1, \ldots, k_n)|^2, \quad \mathcal{M}_0^\lambda = \hat{\beta}_0^\lambda, \\ \mathcal{M}_{1,\sigma_1}^\lambda(k_1) &= \hat{\beta}_0^\lambda \mathbb{S}_{\sigma_1}(k_1) + \hat{\beta}_{1,\sigma_1}^\lambda(k_1), \\ \mathcal{M}_{2,\sigma_1,\sigma_2}^\lambda(k_1, k_2) &= \hat{\beta}_0^\lambda \mathbb{S}_{\sigma_1}(k_1)\mathbb{S}_{\sigma_2}(k_2) + \hat{\beta}_{1,\sigma_1}^\lambda(k_1)\mathbb{S}_{\sigma_2}(k_2) \\ & + \hat{\beta}_{1,\sigma_2}^\lambda(k_2)\mathbb{S}_{\sigma_1}(k_1), \\ \mathcal{M}_{n,\sigma_1,\ldots\sigma_n}^\lambda(k_1, \ldots k_n) &= \hat{\beta}_0^\lambda \mathbb{S}_{\sigma_1}(k_1)\mathbb{S}_{\sigma_2}(k_2)\ldots\mathbb{S}_{\sigma_n}(k_n) \\ & + \hat{\beta}_{1,\sigma_1}^\lambda(k_1)\mathbb{S}_{\sigma_2}(k_2)\ldots\mathbb{S}_{\sigma_n}(k_n) \\ & + \mathbb{S}_{\sigma_1}(k_1)\hat{\beta}_{1,\sigma_2}^\lambda(k_2)\ldots\mathbb{S}_{\sigma_n}(k_n) \\ & + \cdots + \mathbb{S}_{\sigma_1}(k_1)\mathbb{S}_{\sigma_2}(k_2)\ldots \\ & \times \mathbb{S}_{\sigma_{n-1}}(k_{n-1})\hat{\beta}_{1,\sigma_n}^\lambda(k_n), \end{aligned} \quad (4)$$

where λ is the collective index of fermion helicities. The $\mathcal{O}(\alpha^1)$ IR-finite building blocks are

$$\hat{\beta}_0^\lambda = (e^{-\alpha B_4}\mathcal{M}_\lambda^{\text{Born+Virt}})|_{\mathcal{O}(\alpha^1)},$$
$$\hat{\beta}_{1,\sigma}^\lambda(k) = \mathcal{M}_{1,\sigma}^\lambda(k) - \hat{\beta}_0^\lambda \mathbb{S}_\sigma(k)$$

Everything above is expressed in terms of $\mathcal{M}$-amplitudes. Distributions are ≥ 0 by construction. In $\mathcal{KK}$ MC the above is done up to $\mathcal{O}(\alpha^2)$ for ISR and FSR.

The full scale CEEX $\mathcal{O}(\alpha^r)$, $r = 1, 2$, master formula for the polarized total cross section reads as follows:

$$\begin{aligned} \sigma^{(r)} = \sum_{n=0}^{\infty} \frac{1}{n!} \int d\tau_n(p_a + p_b; p_c, p_d, k_1, \ldots, k_n) e^{2\alpha\Re B_4} \\ \times \sum_{\sigma_i, \lambda, \bar{\lambda}} \sum_{i,j,l,m=0}^{3} \hat{\varepsilon}_a^i \hat{\varepsilon}_b^j \sigma_{\lambda_a\bar{\lambda}_a}^i \sigma_{\lambda_b\bar{\lambda}_b}^j \mathfrak{M}_n^{(r)}\begin{pmatrix} pk_1k_2 \ldots k_n \\ \lambda\sigma_1\sigma_2 \ldots \sigma_n \end{pmatrix} \\ \times \left[\mathfrak{M}_n^{(r)}\begin{pmatrix} pk_1k_2 \ldots k_n \\ \bar{\lambda}\sigma_1\sigma_2 \ldots \sigma_n \end{pmatrix}\right]^\star \sigma_{\bar{\lambda}_c\lambda_c}^l \sigma_{\bar{\lambda}_d\lambda_d}^m \hat{h}_c^l \hat{h}_d^m. \end{aligned} \quad (5)$$

The respective CEEX amplitudes are

$$\begin{aligned} \mathfrak{M}_n^{(1)}\begin{pmatrix} pk_1 \ldots k_n \\ \lambda\sigma_1 \ldots \sigma_n \end{pmatrix} &= \sum_{\wp\in\mathcal{P}} \prod_{i=1}^n \mathbb{S}_{[i]}^{\{\wp_i\}} \left\{ \hat{\beta}_0^{(1)}\begin{pmatrix} p \\ \lambda \end{pmatrix}; X_\wp) + \sum_{j=1}^n \frac{\hat{\beta}_{1\{\wp_j\}}^{(1)}(\begin{smallmatrix} pk_j \\ \lambda\sigma_j \end{smallmatrix}; X_\wp)}{\mathbb{S}_{[j]}^{\{\wp_j\}}} \right\} \\ \mathfrak{M}_n^{(2)}\begin{pmatrix} pk_1 \ldots k_n \\ \lambda\sigma_1 \ldots \sigma_n \end{pmatrix} &= \sum_{\wp\in\mathcal{P}} \prod_{i=1}^n \mathbb{S}_{[i]}^{\{\wp_i\}} \left\{ \hat{\beta}_0^{(2)}\begin{pmatrix} p \\ \lambda \end{pmatrix}; X_\wp\right) + \sum_{j=1}^n \frac{\hat{\beta}_{2\{\wp_j\}}^{(1)}(\begin{smallmatrix} pk_j \\ \lambda\sigma_j \end{smallmatrix}; X_\wp)}{\mathbb{S}_{[j]}^{\{\wp_j\}}} \right. \\ & \quad \left. + \sum_{1\leq j<l\leq n} \frac{\hat{\beta}_{2\{\wp_j,\wp_l\}}^{(2)}(\begin{smallmatrix} pk_jk_l \\ \lambda\sigma_j\sigma_l \end{smallmatrix}; X_\wp)}{\mathbb{S}_{[j]}^{\{\wp_j\}} \mathbb{S}_{[l]}^{\{\wp_l\}}} \right\}. \end{aligned} \quad (6)$$

For the full details see Ref. [12].

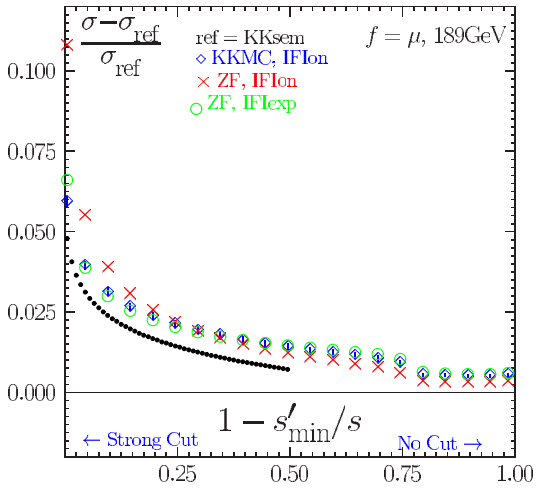

FIG. 1 (color online). Principal cross-checks of $\mathcal{KKMC}$ for $e^-e^+ \to \mu^-\mu^+ + n\gamma$ process at $\sqrt{s} = 189$ GeV.

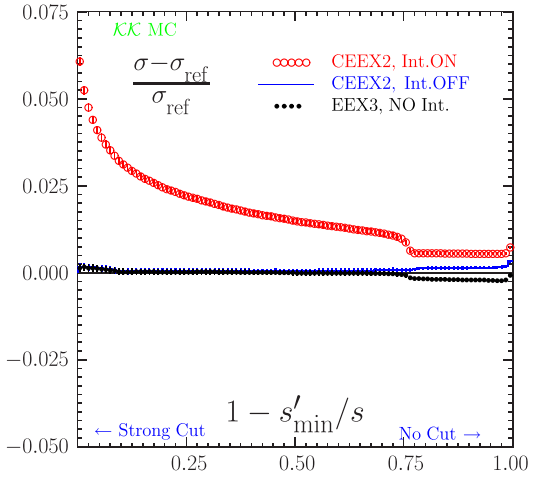

FIG. 2 (color online). Total cross section σ, energy cutoff study. The same results as in Table I. Reference $\sigma_{\rm ref}$ = semianalytical of $\mathcal{KK}$sem.

The precision tags of the $\mathcal{KK}$ MC are determined by comparisons with our own semianalytical and independent MC results and by comparison with the semianalytical results of the program ZFITTER [24]. In Fig. 1 we illustrate such comparisons, which lead to the $\mathcal{KK}$ MC precision tag $d\sigma/\sigma = 0.2\%$ for example. The ISR of ZFITTER is based on the $\mathcal{O}(\alpha^2)$ result of Ref. [25], while $\mathcal{KK}$ MC is totally independent. See Refs. [12,26] for a more complete discussion. Thus, we know that $\mathcal{KK}$ MC has the capability to deliver per mille precision on the large EW effects if it is extended to the appropriate incoming beams for the LHC and the muon collider. To this we now turn.

TABLE I. Energy cutoff study of total cross section σ and charge asymmetry $A_{\rm FB}$ for annihilation process $e^-e^+ \to \mu^-\mu^+$, at $\sqrt{s} = 189$ GeV. Energy cut: $v < v_{\rm max}$, $v = 1 - M^2_{f\bar{f}}/s$. Scattering angle for $A_{\rm FB}$ is $\theta^\bullet$(defined in Phys. Rev. **D41**, 1425 (1990)). No cut in $\theta^\bullet$. EW correction in $\mathcal{KK}$ according to DIZET 6.x. In addition to CEEX matrix element, results are also shown for $\mathcal{O}(\alpha^3)_{\rm LL}$ EEX3 matrix element without ISR ⊗ FSR interference $\mathcal{KK}$sem is semianalytical program, part of $\mathcal{KK}$ MC.

$v_{\rm max}$	$\mathcal{KK}$sem Refer.	$\mathcal{O}(\alpha^3)_{\rm EEX3}$	$\mathcal{O}(\alpha^2)_{\rm CEEX}$ intOFF	$\mathcal{O}(\alpha^2)_{\rm CEEX}$
		$\sigma(v_{\rm max})$ [pb]		
0.01	1.6712 ± 0.0000	1.6736 ± 0.0018	1.6738 ± 0.0018	1.7727 ± 0.0021
0.10	2.5198 ± 0.0000	2.5205 ± 0.0020	2.5210 ± 0.0020	2.6009 ± 0.0024
0.30	3.0616 ± 0.0000	3.0626 ± 0.0022	3.0634 ± 0.0022	3.1243 ± 0.0026
0.50	3.3747 ± 0.0000	3.3745 ± 0.0022	3.3761 ± 0.0022	3.4254 ± 0.0026
0.70	3.7223 ± 0.0000	3.7214 ± 0.0022	3.7249 ± 0.0022	3.7648 ± 0.0027
0.90	7.1430 ± 0.0000	7.1284 ± 0.0022	7.1530 ± 0.0022	7.1821 ± 0.0026
0.99	7.6136 ± 0.0000	7.5974 ± 0.0021	7.6278 ± 0.0021	7.6567 ± 0.0026
		$A_{\rm FB}(v_{\rm max})$		
0.01	0.5654 ± 0.0000	0.5661 ± 0.0012	0.5661 ± 0.0012	0.6121 ± 0.0014
0.10	0.5664 ± 0.0000	0.5667 ± 0.0009	0.5667 ± 0.0009	0.5931 ± 0.0011
0.30	0.5692 ± 0.0000	0.5694 ± 0.0008	0.5693 ± 0.0008	0.5864 ± 0.0010
0.50	0.5744 ± 0.0000	0.5744 ± 0.0008	0.5743 ± 0.0008	0.5870 ± 0.0009
0.70	0.5863 ± 0.0000	0.5858 ± 0.0007	0.5857 ± 0.0007	0.5953 ± 0.0008
0.90	0.3105 ± 0.0000	0.3107 ± 0.0004	0.3100 ± 0.0004	0.3176 ± 0.0004
0.99	0.2851 ± 0.0000	0.2856 ± 0.0003	0.2848 ± 0.0003	0.2918 ± 0.0004

III. EXTENSION OF $\mathcal{KK}$ MC TO THE PROCESSES $f\bar{f} \to f'\bar{f}'$, $f = \mu, q, \nu_\ell$, $f' = \ell, \nu_\ell, q$, $q = u, d, s, c, b$, $\ell = e, \mu, \tau$, $f \neq f'$

At the LHC and at a futuristic muon collider [17], the incoming beams involve for $Z/\gamma*$ production and decay the other light charged fundamental fermions in the SM: u, d, s, c, b for the LHC and the muon for a muon collider. Thus, we need to extend the matrix elements, residuals, and IR functions in (1) and (5) to the case where we substitute the e^-, e^+ EW charges by the new beam particles f, $\bar{f}$ EW charges and we substitute the mass m_e everywhere by m_f.[3] We have done this with considerable cross-checks against the same semianalytical tools that we employed in Ref. [12] to establish the precision tag of version 4.13 of $\mathcal{KK}$ MC. We want to stress that this was a highly nontrivial set of cross-checks: for example, we found that the MC procedure used in the crude MC cross section was unstable when the value of the radiation strength factor $\gamma_f = \frac{2Q_f^2\alpha}{\pi}(\ln(s/m_f^2) - 1)$ becomes too small.[4] This instability was removed and the correct value of the MC crude cross section was verified by semianalytical methods. We therefore did a series of cross-checks/illustrations with the new version of $\mathcal{KK}$ MC, version 4.22, which we now exhibit.

[3]We advise the reader that especially in the QED radiation module KarLud for the ISR in $\mathcal{KKMC}$, see Ref. [13], some of the expressions had Q_e and m_e effectively hardwired into them and these had to all be found and substituted properly.

[4]In the case of the quarks, we will use here the current quark mass values $m_u \cong 5$ MeV and $m_d \cong 10$ MeV following Ref. [27] for our illustrations; we leave these values as user input in general.

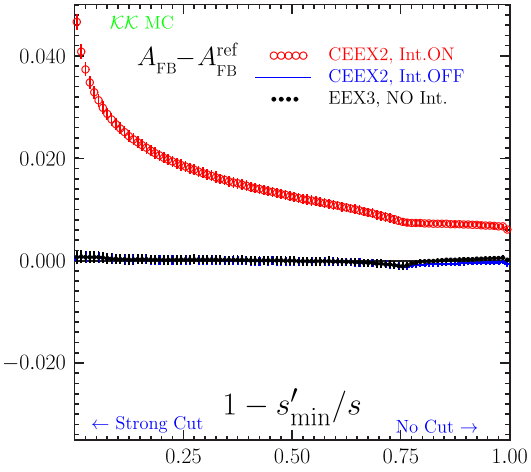

FIG. 3 (color online). Energy cutoff study of charge asymmetry A_{FB} for the process $e^+e^- \to \mu^+\mu^-$. The same results as in Table I. Reference A_{FB}^{ref} = semianalytical $\mathcal{KK}$sem.

Turning first to the most important cross-check, we show in Table I and Figs. 2–4 that for the $e^+e^- \to \mu^+\mu^-$ process, our new version $\mathcal{KK}$ MC 4.22 reproduces the results in the corresponding $\sqrt{s} = 189$ GeV cross-checks done in Ref. [12] for the dependence of the CEEX calculated cross section and A_{FB} on the energy cutoff on $v = 1 - s'/s$ where $s' = M^2_{\mu\bar{\mu}}$ is the invariant mass of the $\mu\bar{\mu}$-system. The reader can check that the two sets of results, those given here in Table I and Figs. 2–4 and those given in Table 5, Figs. 20, 21, and 18 in Ref. [12] are in complete agreement within statistical fluctuations.

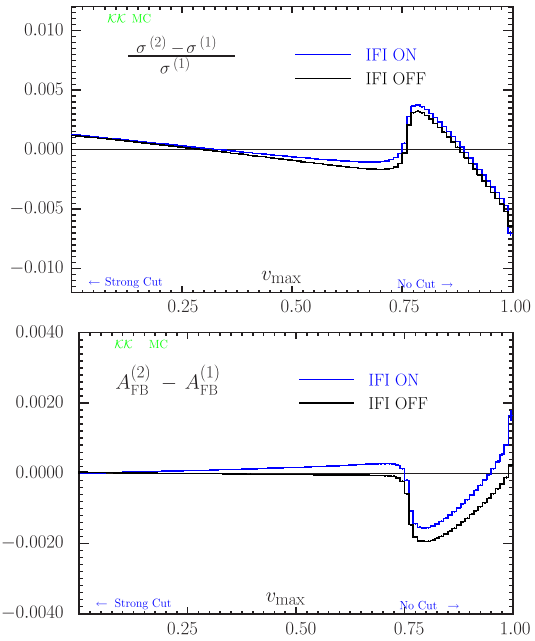

FIG. 4 (color online). Physical precision of CEEX ISR matrix element for $e^-e^+ \to \mu^-\mu^+$ at $\sqrt{s} = 189$ GeV. See Table I for definition of cutoffs.

TABLE II. Study of total cross section $\sigma(v_{max})$ and charge asymmetry $A_{FB}(v_{max})$, $d\bar{d} \to \mu^-\mu^+$, at $\sqrt{s} = 189$ GeV. See Table I for definition of the energy cut v_{max}, scattering angle and M.E. type.

v_{max}	$\mathcal{KK}$sem Refer.	$\mathcal{O}(\alpha^2)_{EEX3}$	$\mathcal{O}(\alpha^2)_{CEEX}$ intOFF	$\mathcal{O}(\alpha^2)_{CEEX}$
		$\sigma(v_{max})$ [pb]		
0.01	0.9145 ± 0.0000	0.9150 ± 0.0004	0.9150 ± 0.0004	0.9323 ± 0.0004
0.10	1.0805 ± 0.0000	1.0807 ± 0.0004	1.0808 ± 0.0004	1.0920 ± 0.0004
0.30	1.1612 ± 0.0000	1.1615 ± 0.0004	1.1616 ± 0.0004	1.1691 ± 0.0004
0.50	1.1974 ± 0.0000	1.1977 ± 0.0004	1.1981 ± 0.0004	1.2036 ± 0.0004
0.70	1.2310 ± 0.0000	1.2312 ± 0.0004	1.2317 ± 0.0004	1.2357 ± 0.0004
0.90	1.6104 ± 0.0000	1.6128 ± 0.0003	1.6114 ± 0.0004	1.6148 ± 0.0004
0.99	1.6218 ± 0.0000	1.6254 ± 0.0003	1.6244 ± 0.0004	1.6277 ± 0.0004
		$A_{FB}(v_{max})$		
0.01	0.5883 ± 0.0000	0.5883 ± 0.0005	0.5883 ± 0.0005	0.6033 ± 0.0005
0.10	0.5882 ± 0.0000	0.5881 ± 0.0004	0.5881 ± 0.0004	0.5966 ± 0.0004
0.30	0.5879 ± 0.0000	0.5879 ± 0.0004	0.5879 ± 0.0004	0.5932 ± 0.0004
0.50	0.5875 ± 0.0000	0.5874 ± 0.0004	0.5875 ± 0.0004	0.5912 ± 0.0004
0.70	0.5848 ± 0.0000	0.5845 ± 0.0004	0.5846 ± 0.0004	0.5868 ± 0.0004
0.90	0.4736 ± 0.0000	0.4722 ± 0.0003	0.4728 ± 0.0003	0.4748 ± 0.0003
0.99	0.4710 ± 0.0000	0.4691 ± 0.0003	0.4697 ± 0.0003	0.4716 ± 0.0003

This shows that our introduction of the new beams has not spoiled the precision of the $\mathcal{KK}$ MC for the incoming e^+e^- state.

We turn next to the new type of incoming beam scenario in Table II and Figs. 5–7 wherein we show the analogous results to those in Table I and Figs. 2–4 for the process $d\bar{d} \to \mu^-\mu^+$ at $\sqrt{s} = 189$ GeV so that we can keep a good reference to the relative size of the EW corrections versus what one would have in the usual e^+e^- annihilation case. We see that for strong cuts, with $v_{max} \sim .01$ and for the loose cut, with $v_{max} \sim 0.99$, the effects are similar to those in the more familiar incoming e^+e^- annihilation case, as the sign of the EW charges are the same for the d and the e^-. The values are different so that size of the

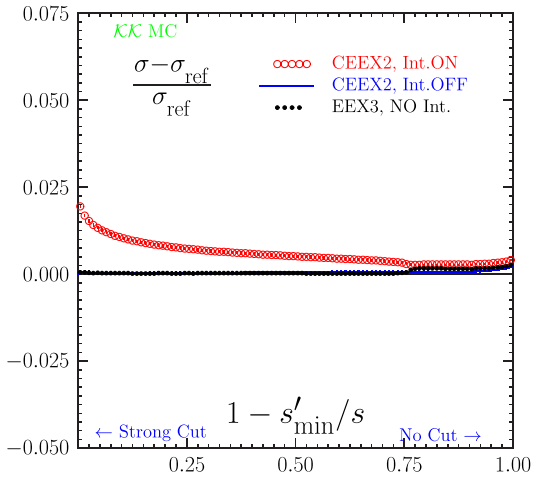

FIG. 5 (color online). Energy cutoff study of total cross section for $d\bar{d} \to \mu^-\mu^+$, at 189 GeV. The same as in Table II. σ_{ref} = semianalytical of $\mathcal{KK}$sem.

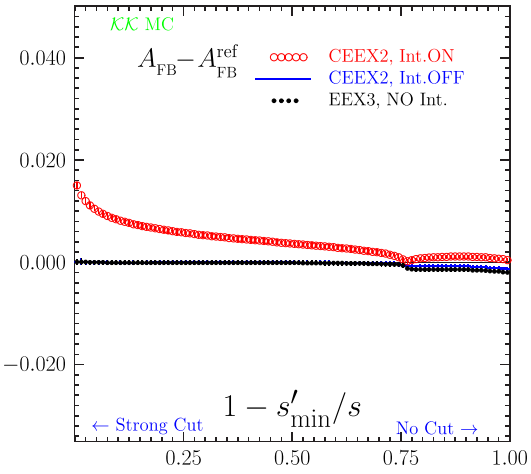

FIG. 6 (color online). Energy cutoff study of charge asymmetry A_{FB} for the process $d\bar{d} \to \mu^- \mu^+$, at 189 GeV. Reference A_{FB}^{ref} from semianalytical $\mathcal{KK}$sem.

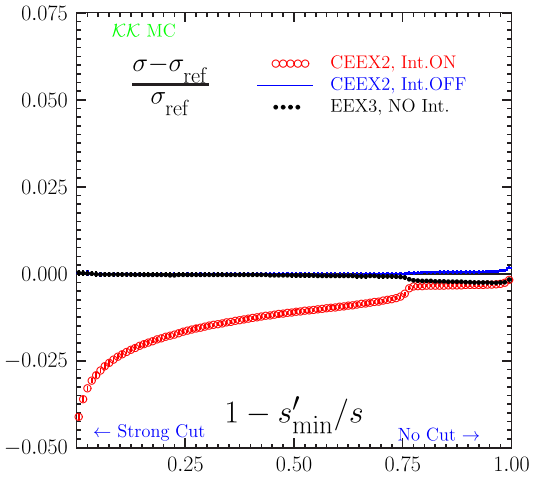

FIG. 8 (color online). Total cross section σ, energy cutoff study for the process $u\bar{u} \to \mu^+ \mu^-$. The same as in the Table III. No cut in $\theta^\bullet$. Reference σ_{ref} = semianalytical of $\mathcal{KK}$sem.

effects in Table II and Figs. 5–7 are correspondingly different. For example, in the strong cut, turning the initial-final state interference(IFI) off changes the CEEX cross section result for $v_{max} = 0.01$ by -1.9% for the incoming $d\bar{d}$ case compared to -5.9% for the incoming $e^- e^+$ case. The behavior of $A_{FB}(v_{max})$ is similar between the two incoming beam sets, where turning the IFI off reduces the value of A_{FB} at $v_{max} = 0.01$ by 8.12%(2.55%), respectively, for the incoming $e^- e^+(d\bar{d})$ case. In both cases, the loose cut such as $v_{max} = 0.99$ tends to wash out these effects. In Fig. 5 the data on the cross sections in Table II are plotted in relation to the reference semianalytical result denoted as $\mathcal{KK}$sem [12] as the ratio of their difference to the reference divided by the reference and in Fig. 6 the corresponding data on A_{FB} are plotted as their difference with the respective $\mathcal{KK}$sem results. When compared to the analogous results for the usual $e^- e^+$ case in Figs. 2 and 3 we see that the structure at the Z-radiative return position, $v_{mas} \cong 0.77$, is very much reduced in the $d\bar{d}$ case due to the smaller electric charge magnitude, just as the size of the IFI effects themselves are similarly reduced. In Fig. 7, we show the physical precision test which compares the size of the second and first order CEEX results for the cross section and the forward-backward asymmetry: for the $d\bar{d}$ case compared to the similar plots in Fig. 4 for the $e^- e^+$ case we see that for the strong cuts we have higher precision, we have smooth behavior through the Z-peak region, and that at the very loose cuts the two precision tags are similar,

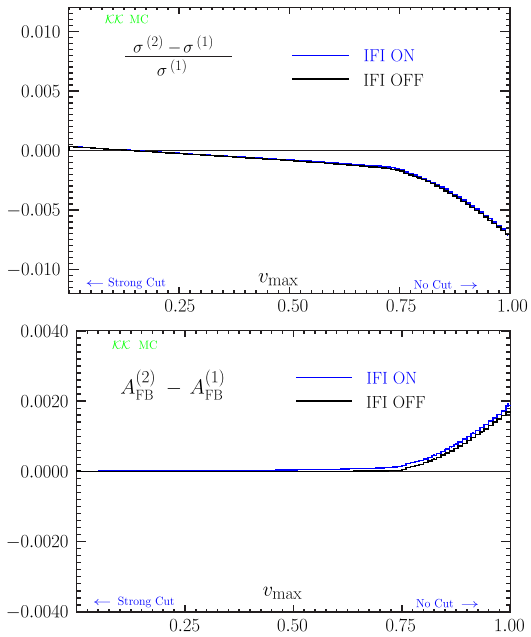

FIG. 7 (color online). Physical precision of CEEX ISR matrix element for $d\bar{d} \to \mu^- \mu^+$ at $\sqrt{s} = 189$ GeV. See Table I for definition of cutoffs.

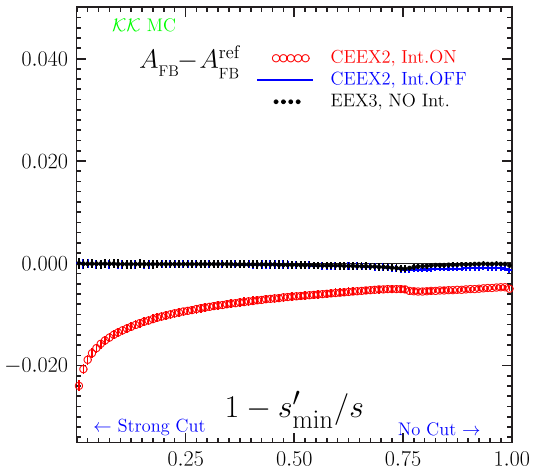

FIG. 9 (color online). Charge asymmetry A_{FB}, energy cutoff study for the process $u\bar{u} \to \mu^+ \mu^-$. The same as in Table III. No cut in $\theta^\bullet$.

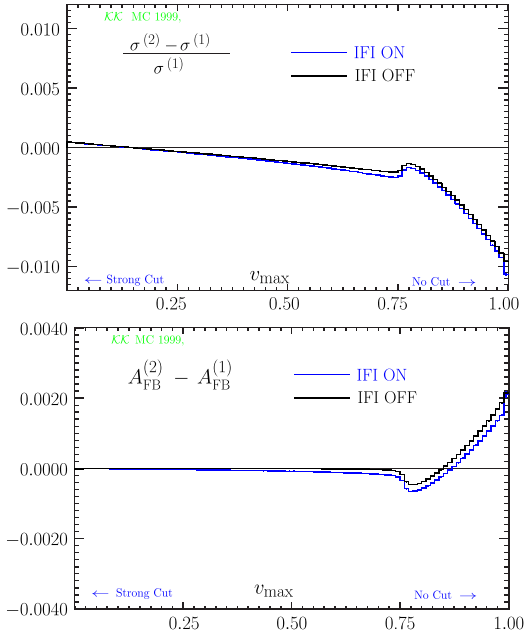

FIG. 10 (color online). Physical precision of CEEX ISR matrix element for $u\bar{u} \to \mu^- \mu^+$ at $\sqrt{s} = 189$ GeV. See Table I for definition of cutoffs.

where we would estimate that similar value at 0.35% in the worst case that $v_{\max} \to 1$ on the cross section for example—here we use half the difference shown in the figure as the error estimate. For the more generic energy cut of 0.6% our physical precision estimate is 0.05%. This is the type of precision required for the precision LHC physics studies.

Turning next to the incoming $u\bar{u}$ case, we show in Table III and Figs. 8–10 the analogous results to those in Table II and Figs. 5–7 for the $u\bar{u} \to \mu^- \mu^+$ at $\sqrt{s} = 189$ GeV, so that again we have the reference to the usual incoming e^+e^- annihilation case regarding the size and nature of the EW effects expected. We see that the effects are now quantitatively different, because the sizes of the EW charges are different, but they also have the opposite sign in the enhanced regions because the EW charges of the u quarks have the opposite sign to those of the e^-. This means that in the LHC environment in processes such as single Z boson production there will be some compensation between the effects from u and d quarks. A detailed application of the new $\mathcal{KK}$ MC two such scenarios will

TABLE III. Study of total cross section $\sigma(v_{\max})$ and charge asymmetry $A_{\rm FB}(v_{\max})$, $u\bar{u} \to \mu^- \mu^+$, at $\sqrt{s} = 189$ GeV. See Table I for definition of the energy cut $v_{\max}$, scattering angle and M.E. type.

$v_{\max}$	$\mathcal{KK}$sem Refer.	$\mathcal{O}(\alpha^2)_{\rm EEX3}$	$\mathcal{O}(\alpha^2)_{\rm CEEX}$ intOFF	$\mathcal{O}(\alpha^2)_{\rm CEEX}$
		$\sigma(v_{\max})$ [pb]		
0.01	1.2714 ± 0.0000	1.2718 ± 0.0009	1.2718 ± 0.0009	1.2191 ± 0.0009
0.10	1.6178 ± 0.0000	1.6175 ± 0.0010	1.6175 ± 0.0010	1.5792 ± 0.0010
0.30	1.8058 ± 0.0000	1.8053 ± 0.0010	1.8054 ± 0.0010	1.7784 ± 0.0010
0.50	1.9026 ± 0.0000	1.9018 ± 0.0010	1.9021 ± 0.0010	1.8815 ± 0.0011
0.70	2.0099 ± 0.0000	2.0084 ± 0.0010	2.0094 ± 0.0010	1.9938 ± 0.0011
0.90	3.3101 ± 0.0000	3.3023 ± 0.0010	3.3120 ± 0.0010	3.2993 ± 0.0010
0.99	3.3961 ± 0.0000	3.3881 ± 0.0010	3.3995 ± 0.0010	3.3872 ± 0.0010
		$A_{\rm FB}(v_{\max})$		
0.01	0.6788 ± 0.0000	0.6787 ± 0.0009	0.6787 ± 0.0009	0.6548 ± 0.0009
0.10	0.6791 ± 0.0000	0.6790 ± 0.0008	0.6790 ± 0.0008	0.6656 ± 0.0008
0.30	0.6799 ± 0.0000	0.6798 ± 0.0007	0.6798 ± 0.0007	0.6713 ± 0.0007
0.50	0.6809 ± 0.0000	0.6806 ± 0.0007	0.6806 ± 0.0007	0.6743 ± 0.0007
0.70	0.6800 ± 0.0000	0.6794 ± 0.0006	0.6793 ± 0.0006	0.6749 ± 0.0007
0.90	0.4417 ± 0.0000	0.4415 ± 0.0004	0.4407 ± 0.0004	0.4366 ± 0.0004
0.99	0.4285 ± 0.0000	0.4283 ± 0.0004	0.4274 ± 0.0004	0.4238 ± 0.0004

TABLE IV. Study of total cross section $\sigma(v_{\max})$ and charge asymmetry $A_{\rm FB}(v_{\max})$, $d\bar{d} \to \mu^- \mu^+$, at $\sqrt{s} = 91.187$ GeV. See Table I for definition of the energy cut $v_{\max}$, scattering angle and M.E. type.

$v_{\max}$	$\mathcal{KK}$sem Refer.	$\mathcal{O}(\alpha^2)_{\rm EEX3}$	$\mathcal{O}(\alpha^2)_{\rm CEEX}$ intOFF	$\mathcal{O}(\alpha^2)_{\rm CEEX}$
		$\sigma(v_{\max})$ [pb]		
0.01	2265.5701 ± 0.0000	2265.7449 ± 0.1721	2265.7796 ± 0.1721	2267.2517 ± 0.1796
0.10	2602.0228 ± 0.0000	2602.4244 ± 0.1519	2602.3968 ± 0.1520	2602.3923 ± 0.1620
0.30	2745.7157 ± 0.0000	2745.9432 ± 0.1385	2746.0304 ± 0.1387	2745.9989 ± 0.1500
0.50	2801.7613 ± 0.0000	2801.7212 ± 0.1317	2802.1262 ± 0.1324	2802.0849 ± 0.1443
0.70	2832.7832 ± 0.0000	2832.3374 ± 0.1275	2833.2354 ± 0.1286	2833.1826 ± 0.1409
0.90	2852.5000 ± 0.0000	2851.5051 ± 0.1246	2853.0535 ± 0.1262	2852.9951 ± 0.1388
0.99	2858.8368 ± 0.0000	2857.5479 ± 0.1237	2859.4417 ± 0.1254	2859.3787 ± 0.1381
		$A_{\rm FB}(v_{\max})$		
0.01	0.1034 ± 0.0000	0.1033 ± 0.0001	0.1033 ± 0.0001	0.1090 ± 0.0001
0.10	0.1032 ± 0.0000	0.1031 ± 0.0001	0.1031 ± 0.0001	0.1034 ± 0.0001
0.30	0.1031 ± 0.0000	0.1031 ± 0.0001	0.1031 ± 0.0001	0.1031 ± 0.0001
0.50	0.1031 ± 0.0000	0.1031 ± 0.0001	0.1031 ± 0.0001	0.1031 ± 0.0001
0.70	0.1031 ± 0.0000	0.1031 ± 0.0001	0.1031 ± 0.0001	0.1031 ± 0.0001
0.90	0.1031 ± 0.0000	0.1030 ± 0.0001	0.1031 ± 0.0001	0.1030 ± 0.0001
0.99	0.1031 ± 0.0000	0.1030 ± 0.0001	0.1030 ± 0.0001	0.1030 ± 0.0001

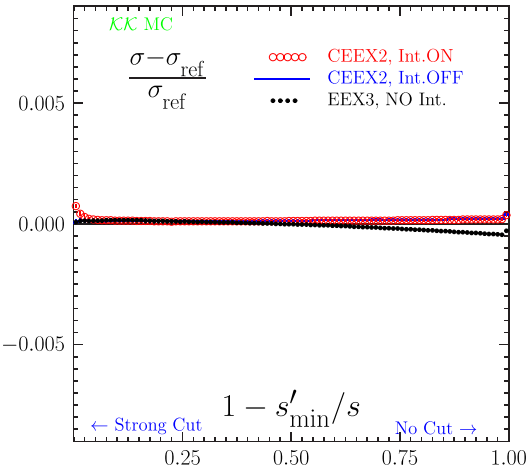

FIG. 11 (color online). Total cross section σ, energy cutoff study for the process $d\bar{d} \to \mu^-\mu^+$ at the Z. Results the same as in Table IV.

appear elsewhere. Here, we specifically note that for the strong cut case with $v_{\rm max} = 0.01$ the IFI effect on the cross section in Table III is -4.14% while the effect on A_{FB} at this value of $v_{\rm max}$ is -3.52%, both of which correlate well with the value of the u-quark EW charges compared to the e^- EW charges, where the corresponding results are from Table I 5.9% and 8.12%, respectively. In Figs. 8 and 9 we show for the incoming $u\bar{u}$ the analogous plots to those in Figs. 5 and 6 for the incoming $d\bar{d}$ case of the relative values of the data in Table III. We see that the structure at the Z-radiative return position is a bit more evident than for the latter case and that the IFI effects are correspondingly more evident in general, as expected. In Fig. 10, we show the corresponding physical precision study as the difference between the second and first order CEEX predictions. In the worst case scenario with $v_{\rm max} \to 1$ we have the estimate at 0.5% on the cross section; at strong cuts $v_{\rm max} \to 0$

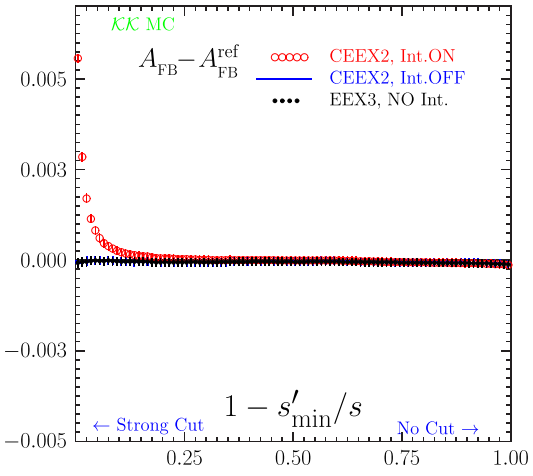

FIG. 12 (color online). Charge asymmetry $A_{\rm FB}$, energy cutoff study for the process $d\bar{d} \to \mu^-\mu^+$ at the Z. Results the same as in Table IV.

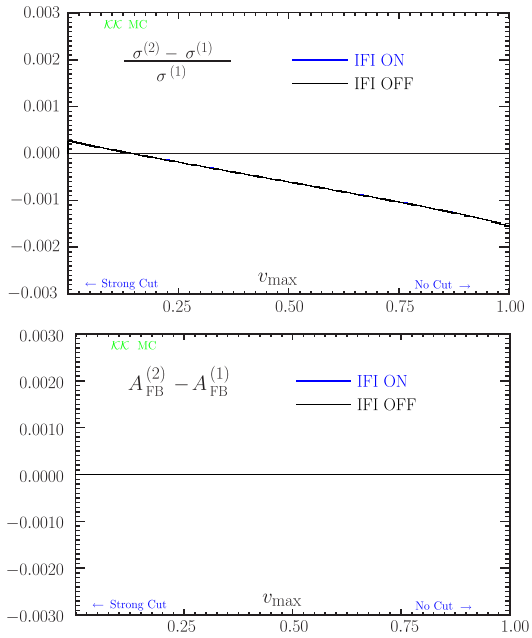

FIG. 13 (color online). Physical precision of CEEX ISR matrix element for $d\bar{d} \to \mu^-\mu^+$ at $\sqrt{s} = 91.187$ GeV. See Table I for definition of cutoffs.

we have 0.025% and at moderate cuts near $v_{\rm max} \cong 0.6$ we have .08%, as needed for precision LHC studies. These estimates hold for both the IFI on and IFI off cases.

As most of the cross section at the LHC in the single $Z/\gamma*$ production and decay to lepton pairs is concentrated near the Z-resonance, we next turn to the similar studies as we have shown in Tables I, II, and III and Figs. 2–10 for $\sqrt{s} = M_Z$ so we see more directly what type of effects one has to consider in precision studies of these processes. We stress that with 25 fb^{-1} of recorded data for each of ATLAS and CMS, the number of such decays exceeds 10 M in each experiment. Turning first to the $d\bar{d}$ incoming beam scenario we have the results in Table IV and Figs. 11–13. We see that the small width(that is to say the lifetime) of the Z suppresses the IFI effects as expected: on the cross section even for the strong cut $v_{\rm max} = 0.01$ the effect is at the level of only 0.065% and it is already essentially nonexistent at $v_{\rm max} = 0.1$; on A_{FB} a 5.5% enhancement at $v_{\rm max} = 0.01$ is already reduced to 0.29% at $v_{\rm max} = 0.1$. But, the effect of the radiation on the cross section is quite pronounced, as the cross section changes by 26% between the strong cut $v_{\rm max} = 0.01$ and the loose cut $v_{\rm max} = 0.99$. Thus, high precision on its theoretical prediction is essential for LHC precision studies. Indeed, these remarks are borne out in the plots in Figs. 11 and 12, where we respectively see the closeness of the CEEX cross section with the IFI on and IFI off and the similar closeness of the CEEX forward-backward asymmetries with the IFI on and off except for the region below $v_{\rm max} = 0.01$, where the IFI effect reaches 5.5%. Turning to the physical precision study in Fig. 13, we see that in the typical scenario

TABLE V. Study of total cross section $\sigma(v_{\max})$ and charge asymmetry $A_{\rm FB}(v_{\max})$, $u\bar{u} \to \mu^-\mu^+$, at $\sqrt{s} = 91.187$ GeV. See Table I for definition of the energy cut $v_{\max}$, scattering angle and M.E. type.

$v_{\max}$	$\mathcal{KK}$sem Refer.	$\mathcal{O}(\alpha^2)_{\rm EEX3}$	$\mathcal{O}(\alpha^2)_{\rm CEEX}$ intOFF	$\mathcal{O}(\alpha^2)_{\rm CEEX}$
		$\sigma(v_{\max})$ [pb]		
0.01	1564.0869 ± 0.0000	1564.5424 ± 0.2794	1564.5808 ± 0.2794	1563.6629 ± 0.3001
0.10	1854.9598 ± 0.0000	1855.4516 ± 0.2453	1855.4499 ± 0.2453	1855.4759 ± 0.2771
0.30	1959.9902 ± 0.0000	1960.2774 ± 0.2250	1960.3844 ± 0.2252	1960.3109 ± 0.2610
0.50	2000.3461 ± 0.0000	2000.4857 ± 0.2150	2000.8275 ± 0.2155	2000.7314 ± 0.2530
0.70	2022.6577 ± 0.0000	2022.5082 ± 0.2087	2023.2161 ± 0.2095	2023.1098 ± 0.2482
0.90	2036.8954 ± 0.0000	2036.3586 ± 0.2044	2037.5580 ± 0.2055	2037.4527 ± 0.2449
0.99	2041.6520 ± 0.0000	2040.9151 ± 0.2030	2042.3715 ± 0.2042	2042.2608 ± 0.2439
		$A_{\rm FB}(v_{\max})$		
0.01	0.0736 ± 0.0000	0.0732 ± 0.0003	0.0732 ± 0.0003	0.0613 ± 0.0003
0.10	0.0712 ± 0.0000	0.0708 ± 0.0002	0.0708 ± 0.0002	0.0701 ± 0.0003
0.30	0.0708 ± 0.0000	0.0703 ± 0.0002	0.0703 ± 0.0002	0.0701 ± 0.0002
0.50	0.0707 ± 0.0000	0.0702 ± 0.0002	0.0702 ± 0.0002	0.0701 ± 0.0002
0.70	0.0706 ± 0.0000	0.0702 ± 0.0002	0.0702 ± 0.0002	0.0702 ± 0.0002
0.90	0.0706 ± 0.0000	0.0702 ± 0.0002	0.0702 ± 0.0002	0.0702 ± 0.0002
0.99	0.0706 ± 0.0000	0.0701 ± 0.0002	0.0701 ± 0.0002	0.0701 ± 0.0002

where $v_{\max} \cong 0.6$, the precision tag for both IFI on and the IFI off cross sections is 0.04%, sufficient for the precision LHC studies.

Continuing in this vein, we present next the incoming $u\bar{u}$ scenario at $\sqrt{s} = M_Z$ in Table V and Figs. 14–16. We see again that the small width of the Z suppresses the IFI effects: the negative effects at $v_{\max} = 0.01$ of -0.0587% on the cross section and -16.2% on A_{FB} become, respectively, nonexistent and $-.989\%$ at $v_{\max} = 0.1$; at the loose cut $v_{\max} = 0.99$ the IFI effect on the cross section (the forward-backward asymmetry) is below the 0.01% (0.00285) precision of the data. The cross section varies by 30.6% as $v_{\max}$ varies from 0.01 to 0.99 so again its theoretical prediction for the radiative effects must have high precision for precision studies. These remarks are borne out by the plots in Figs. 14 and 15, where we see that the IFI on and IFI CEEX cross sections are very close to the reference cross section even for the very strong and loose cuts and that the IFI on and off CEEX forward-backward asymmetries are the same as the EEX3 value by an energy cut value of 0.25, for example. In Fig. 16, we see the precision study shows that the cross section has the precision estimate of 0.04% at the energy cut of 0.6 just as we had for the incoming $d\bar{d}$ case. Again, this is sufficient for precision studies of LHC physics.

While we have discussed the individual incoming $q\bar{q}$ scenarios, $\mathcal{KK}$ MC 4.22 has a beamstrahlung option in which one may replace the beamstrahlung functions with

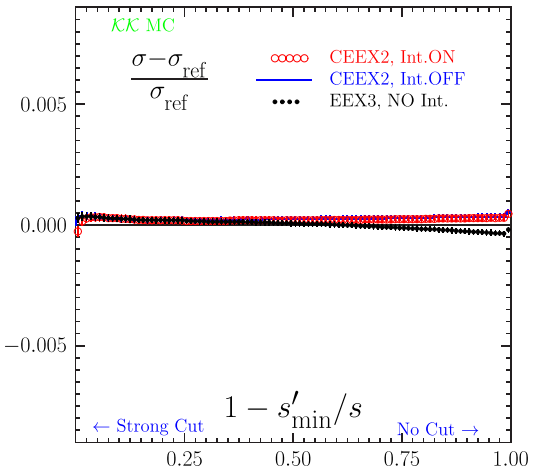

FIG. 14 (color online). Total cross section σ, energy cutoff study for the process $u\bar{u} \to \mu^+\mu^-$ at the Z peak. Results the same as in Table V.

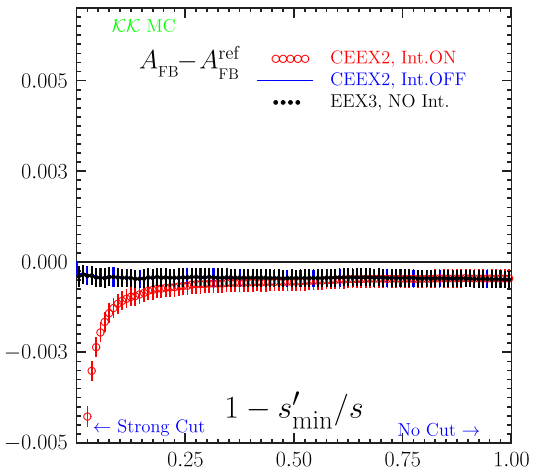

FIG. 15 (color online). Charge asymmetry $A_{\rm FB}$, energy cutoff study for the process $u\bar{u} \to \mu^-\mu^+$ at the Z. Results the same as in Table V.

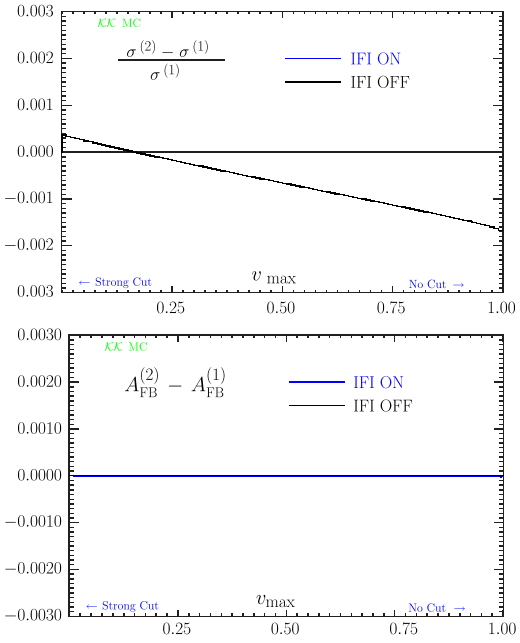

FIG. 16 (color online). Physical precision of CEEX ISR matrix element for $u\bar{u} \to \mu^-\mu^+$ at $\sqrt{s} = 91.187$ GeV(Z peak). See Table I for definition of cutoffs.

the proton PDF's. We have done this as a proof of principle exercise and we show in Appendix A the results of a simple test run at 7 TeV. What we see in this test run output is that indeed significant probability exists for the incoming quarks to radiate nonzero p_T in the higher order corrections: these effects cannot be properly described by zero p_T methods such as structure function techniques [4]. We will return to such studies elsewhere [21].

Finally, given the interest in muon collider precision physics [17], we consider next the process $\mu^+\mu^- \to e^+e^-$

TABLE VI. Study of total cross section $\sigma(v_{\max})$ and charge asymmetry $A_{\rm FB}(v_{\max})$, $\mu^-\mu^+ \to e^-e^+$, at $\sqrt{s} = 189$ GeV. See Table I for definition of the energy cut $v_{\max}$, scattering angle and M.E. type.

$v_{\max}$	$\mathcal{KK}$sem Refer.	$\mathcal{O}(\alpha^2)_{\rm EEX3}$	$\mathcal{O}(\alpha^2)_{\rm CEEX}$ intOFF	$\mathcal{O}(\alpha^2)_{\rm CEEX}$
		$\sigma(v_{\max})$ [pb]		
0.01	1.6703 ± 0.0000	1.6716 ± 0.0040	1.6718 ± 0.0040	1.7721 ± 0.0048
0.10	2.5076 ± 0.0000	2.5119 ± 0.0046	2.5123 ± 0.0046	2.5946 ± 0.0055
0.30	3.0153 ± 0.0000	3.0192 ± 0.0048	3.0203 ± 0.0048	3.0813 ± 0.0057
0.50	3.2808 ± 0.0000	3.2839 ± 0.0049	3.2867 ± 0.0049	3.3348 ± 0.0058
0.70	3.5252 ± 0.0000	3.5277 ± 0.0049	3.5338 ± 0.0049	3.5712 ± 0.0059
0.90	5.4288 ± 0.0000	5.3946 ± 0.0047	5.4412 ± 0.0047	5.4699 ± 0.0057
0.99	5.7248 ± 0.0000	5.6824 ± 0.0046	5.7414 ± 0.0046	5.7697 ± 0.0057
		$A_{\rm FB}(v_{\max})$		
0.01	0.5654 ± 0.0000	0.5664 ± 0.0028	0.5664 ± 0.0028	0.6132 ± 0.0032
0.10	0.5659 ± 0.0000	0.5666 ± 0.0021	0.5666 ± 0.0021	0.5934 ± 0.0025
0.30	0.5675 ± 0.0000	0.5684 ± 0.0019	0.5684 ± 0.0019	0.5855 ± 0.0022
0.50	0.5705 ± 0.0000	0.5710 ± 0.0018	0.5710 ± 0.0018	0.5835 ± 0.0021
0.70	0.5774 ± 0.0000	0.5776 ± 0.0017	0.5777 ± 0.0017	0.5870 ± 0.0020
0.90	0.3844 ± 0.0000	0.3873 ± 0.0011	0.3848 ± 0.0011	0.3921 ± 0.0012
0.99	0.3613 ± 0.0000	0.3652 ± 0.0010	0.3622 ± 0.0010	0.3683 ± 0.0012

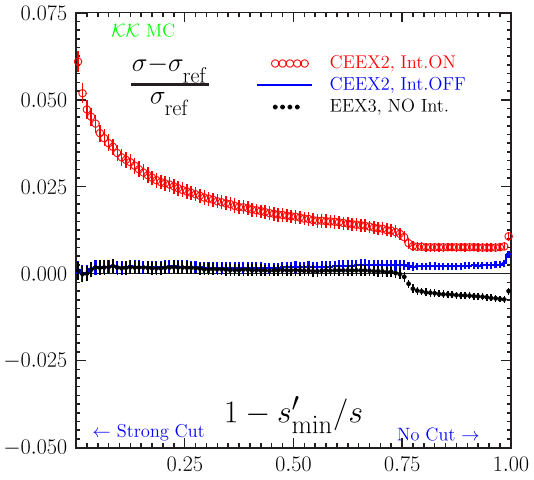

FIG. 17 (color online). Energy cutoff study of total cross section for $\mu^-\mu^+ \to e^-e^+$ at energy 189 GeV. The same results as in Table VI.

again at $\sqrt{s} = 189$ GeV, so that again we have the reference to the usual incoming e^+e^- annihilation case regarding the size and nature of the EW effects expected. In this case we have all the same EW charges but the ISR probability to radiate factor $\gamma_e = \frac{2\alpha}{\pi}(\ln(s/m_e^2) - 1) \cong 0.114$ becomes $\gamma_\mu = \frac{2\alpha}{\pi}(\ln(s/m_\mu^2) - 1) \cong 0.0649$. This means that we expect the EW effects where the photonic corrections dominate to show reduction in size for ISR dominated regimes, the same size for the IFI dominated regimes. This is borne out by the results in Table VI and Figs. 17–19. In the regime of the strong cut, with $v_{\max} = 0.01$, the results are very similar in all aspects to the usual incoming e^-e^+ case: the cross section is enhanced by 6.0% to be compared with 5.9% and A_{FB} is enhanced by 8.3% to be compared to 8.1%. In the regime of the loose cut, with $v_{\max} = 0.99$, the cross section is enhanced by 0.49% to be compared with 0.38% and A_{FB} is enhanced by 1.7% to be compared to

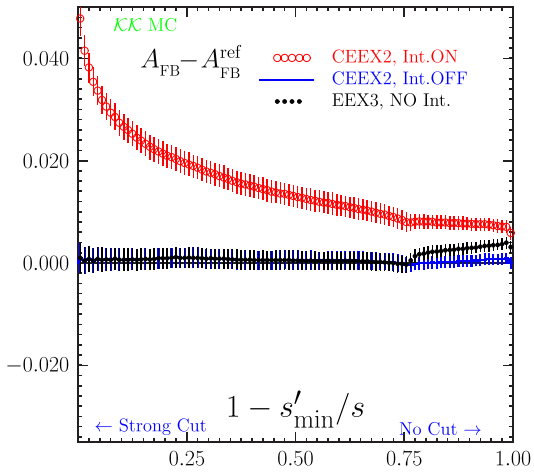

FIG. 18 (color online). Energy cutoff study of total charge asymmetry for $\mu^-\mu^+ \to e^-e^+$ at energy 189 GeV. The same results as in Table VI.

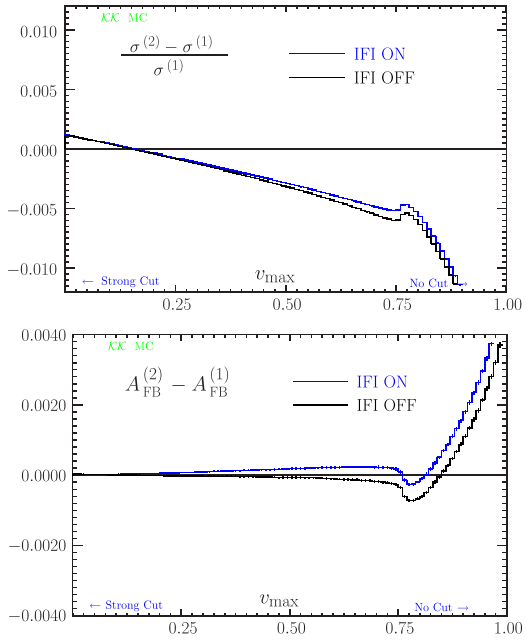

FIG. 19 (color online). Physical precision of CEEX ISR matrix element for $\mu^-\mu^+ \to e^-e^+$ at $\sqrt{s} = 189$ GeV. See Table I for definition of cut-offs.

2.4%. In Figs. 17 and 18 we see that we have same general behavior as we have in Figs. 2 and 3, the characteristic Z peak radiative return structure in Fig. 17 and its inflection behavior in Fig. 18. In Fig. 19, we see that the precision studies comparing the second order and first order CEEX results show the pronounced effect of the Z radiative return. At an energy cut of 0.6, we see again that a precision tag of 0.2% obtains, so that precision results for EW effects would be available. The detailed application of such results to muon collider physics will be taken up elsewhere [28].

IV. CONCLUSIONS

YFS inspired EEX and CEEX MC schemes are successful examples of Monte Carlos based directly on the factorization theorem (albeit for the IR soft case for Abelian QED only). These schemes work well in practice: KORALZ, BHLUMI, YWSWW3, BHWIDE and $\mathcal{KK}$ MC are examples. The extension of such schemes (as far as possible) to all collinear singularities would be very desirable and practically important. Work on this is in progress—see Refs. [29–31] for recent results and outlooks.

Here, we have illustrated that the $\mathcal{KK}$ MC program is extended to the new incoming $f\bar{f}$, $f = \mu, \tau, \nu_\ell, q, q = u, d, s, c, b, \ell = e, \mu, \tau$, beams cases. The quark-antiquark and $\mu^-\mu^+$ incoming beam cases are, respectively, important for the LHC precision EW predictions at the per mille level and to the precision EW studies for the possible muon collider physics program. We have seen that in all cases, the per mille level accuracy requirements necessitate the implementation of the $\mathcal{KK}$ MC class of EW higher order effects. Realizations and applications of this class of higher order EW effects is in progress and will appear elsewhere [21]. The new version of the $\mathcal{KK}$ MC, version 4.22, is available at https://jadach.web.cern.ch/jadach/KKindex.html.

ACKNOWLEDGMENTS

The authors thank Prof. I. Antoniadis for the support and kind hospitality of the CERN Theory Division while this work was in progress. They also thank Dr. S. A. Yost for useful discussions. One of the authors (S. J.) also thanks Dean Lee Nordt of the Baylor College of Arts & Sciences for Baylor's support while this work was in progress. This work is partly supported by the Polish National Science Centre Grant No. DEC-2011/03/B/ST2/02632.

APPENDIX: SAMPLE MONTE CARLO EVENTS

Below sample output from run of $\mathcal{KK}$ MC version 4.22 is presented for $pp \to u\bar{u} \to l^-l^+ + n\gamma$ where simple parton distribution functions (PDF's) of u and $\bar{u}$ quarks in the proton are replacing beamstrahlung distributions (see function BORNV_RHOFOAMC in the source code). Three events are shown in the popular LUND MC format. Two photons in the event record with the exactly zero transverse momentum, formerly beamstrahlung photons, are now representing proton remnants (temporary fix). What is important to see is the perfect energy momentum conservation and proper flavor structure. Overall normalization of the cross section is in principle also under strict control, however, more tests are needed.

KK Monte Carlo

Version	4.22	May 2013		
7000.00000000		CMS energy average	CMSene	a1
0.00000000		Beam energy spread	DelEne	a2
100		Max. photon mult.	npmax	a3
0		wt-ed or wt = 1 evts.	KeyWgt	a4
1		ISR switch	KeyISR	a4
1		FSR switch	KeyFSR	a5
2		ISR/FSR interferenc	KeyINT	a6
1		New exponentiation	KeyGPS	a7
0		Hadroniz. switch	KeyHad	a7
0.20000000		Hadroniz. min. mass	HadMin	a9
1.00000000		Maximum weight	WTmax	a10
100		Max. photon mult.	npmax	a11
2		Beam ident	KFini	a12
0.03500000		Manimum phot. ener.	Ene	a13
0.10000000E-59		Phot.mass, IR regul	MasPho	a14
1.2500000		Phot. mult. enhanc.	Xenph	a15
0.00000000		PolBeam1(1)	Pol1x	a17
0.00000000		PolBeam1(2)	Pol1y	a18
0.00000000		PolBeam1(3)	Pol1z	a19
0.00000000		PolBeam2(1)	Pol2x	a20
0.00000000		PolBeam2(2)	Pol2y	a21
0.00000000		PolBeam2(3)	Pol2z	a22

Event listing (summary)

I	particle/jet	KS	KF	orig	p_x	p_y	p_z	E	m
1	!u!	21	2	0	0.000	0.000	22.668	22.668	0.005
2	!ubar!	21	−2	0	0.000	0.000	−245.458	245.458	0.005
3	(Z0)	11	23	1	23.016	18.370	−80.068	115.249	77.487
4	gamma	1	22	1	−30.989	−6.132	−128.905	132.719	0.000
5	gamma	1	22	1	0.000	0.000	0.031	0.031	0.000
6	gamma	1	22	1	7.973	−12.238	−13.848	20.127	0.000
7	gamma	1	22	1	0.000	0.000	3477.332	3477.332	0.000
8	gamma	1	22	1	0.000	0.000	−3254.542	3254.542	0.000
9	tau−	1	15	3	−24.701	21.657	−20.217	38.613	1.777
10	tau+	1	−15	3	47.716	−3.287	−59.851	76.635	1.777
		sum:	0.00		0.000	0.000	0.000	7000.000	7000.000

Event listing (summary)

I	particle/jet	KS	KF	orig	p_x	p_y	p_z	E	m
1	!u!	21	2	0	0.000	0.000	271.908	271.908	0.005
2	!ubar!	21	−2	0	0.000	0.000	−6.542	6.542	0.005
3	(Z0)	11	23	1	0.047	1.133	244.401	257.454	80.928
4	gamma	1	22	1	−0.047	−1.133	20.965	20.996	0.000
5	gamma	1	22	1	0.000	0.000	3228.092	3228.092	0.000
6	gamma	1	22	1	0.000	0.000	−3493.458	3493.458	0.000
7	mu−	1	13	3	0.601	14.537	2.005	14.687	0.106
8	mu+	1	−13	3	−0.554	−13.404	242.396	242.767	0.106
		sum:	0.00		0.000	0.000	0.000	7000.000	7000.000

Event listing (summary)

I	particle/jet	KS	KF	orig	p_x	p_y	p_z	E	m
1	!u!	21	2	0	0.000	0.000	1816.851	1816.851	0.005
2	!ubar!	21	−2	0	0.000	0.000	−1.137	1.137	0.005
3	(Z0)	11	23	1	0.011	0.003	1810.259	1812.532	90.760
4	gamma	1	22	1	−0.012	−0.002	5.371	5.371	0.000
5	gamma	1	22	1	0.000	0.000	1683.149	1683.149	0.000
6	gamma	1	22	1	0.000	0.000	−3498.863	3498.863	0.000
7	mu−	1	13	3	12.468	−25.466	1612.743	1612.992	0.106
8	mu+	1	−13	3	−12.457	25.469	197.516	199.540	0.106
		sum:	0.00		−0.001	0.001	−0.084	6999.916	6999.916

KK2f_Finalize printouts

7000.00000000	cms energy total	cmsene	a0
5000	total no of events	nevgen	a1
	** principal info on x-section **		
233.95163953 ±1.04896414	xs_tot MC R-units	xsmc	a1
0.41468908	xs_tot picob.	xSecPb	a3
0.00185933	error picob.	xErrPb	a4
0.00448368	relative error	erel	a5
0.82048782	WTsup, largest WT	WTsup	a10
	** some auxiliary info **		
0.00219522	xs_born picobarns	xborn	a11
0.73760000	Raw phot. multipl.		===
5.00000000	Highest phot. mult.		===
	End of KK2f Finalize		

[1] B. F. L. Ward, Acta Phys. Pol. B **42**, 1663 (2011), and references therein.

[2] S. Jadach and B. F. L. Ward, Phys. Rev. D **38**, 2897 (1988); **39**, 1472 (1989); **40**, 3582 (1989); S. Jadach, B. F. L. Ward, and Z. Was, Comput. Phys. Commun. **66**, 276 (1991); S. Jadach and B. F. L. Ward, Phys. Lett. B **274**, 470 (1992); S. Jadach, E. Richter-Was, B. F. L. Ward, and Z. Was, Comput. Phys. Commun. **70**, 305 (1992); S. Jadach, B. F. L. Ward, and Z. Was, Comput. Phys. Commun. **79**, 503 (1994); S. Jadach, E. Richter-Was, B. F. L. Ward, and Z. Was, Phys. Lett. B **353**, 362 (1995); S. Jadach, E. Richter-Was, B. F. L. Ward, and Z. Was, Phys. Lett. B **384**, 488 (1996); S. Jadach, W. Płaczek, E. Richter-Was, B. F. L. Ward, and Z. Was, Comput. Phys. Commun. **102**, 229 (1997); S. Jadach, W. Placzek, and B. F. L. Ward, Phys. Lett. B **390**, 298 (1997); Phys. Rev. D **54**, 5434 (1996); **56**, 6939 (1997); S. Jadach, M. Skrzypek, and B. F. L. Ward, Phys. Rev. D **55**, 1206 (1997); See, for example, S. Jadach, W. Płaczek, M. Skrzypek, B. F. L. Ward, and Z. Was, Phys. Lett. B **417**, 326 (1998); S. Jadach, W. Płaczek, M. Skrzypek, B. F. L. Ward, and Z. Wąss, Comput. Phys. Commun. **119**, 272 (1999); S. Jadach, W. Płaczek, M. Skrzypek, B. Ward, and Z. Was, Phys. Rev. D **61**, 113010 (2000); S. Jadach, W. Płaczek, M. Skrzypek, B. Ward, and Z. Was, Phys. Rev. D **65**, 093010 (2002); S. Jadach, W. Płaczek, M. Skrzypek, B. F. L. Ward, and Z. Was, Comput. Phys. Commun. **140**, 432 (2001); S. Jadach, W. Płaczek, M. Skrzypek, B. F. L. Ward, and Z. Was, Comput. Phys. Commun. **140**, 475 (2001); S. Jadach, B. F. L. Ward, and Z. Was, Comput. Phys. Commun. **124**, 233 (2000); and references therein.

[3] D. Bardin, S. Bondarenko, P. Christova, L. Kalinovskaya, L. Rumyantsev, A. Sapronov, and W. von Schlippe, JETP Lett. **96**, 285 (2012); D. Bardin *et al.*, arXiv:1207.4400; S. G. Bondarenko and A. A. Sapronov, Comput. Phys. Commun. **184**, 2343 (2013), and references therein.

[4] L. Barzè, G. Montagna, P. Nason, O. Nicrosini, F. Piccinini, and A. Vicini, Eur. Phys. J. C **73**, 2474 (2013); C. M. Carloni-Calame, G. Montagna, O. Nicrosini, and M. Treccani, J. High Energy Phys. 05 (2005) 019; G. Balossini, C. M. Carloni-Calame, G. Montagna, M. Moretti, O. Nicrosini, F. Piccinini, M. Treccani, and A. Vicini, J. Phys. Conf. Ser. **110**, 042002 (2008), and references therein.

[5] Y. Li and F. Petriello, Phys. Rev. D **86**, 094034 (2012).

[6] V. A. Zykunov, Eur. Phys. J. C **3**, 9 (2001); S. Dittmaier and M. Kramer, Phys. Rev. D **65**, 073007 (2002); S. Dittmaier and M. Huber, J. High Energy Phys. 01 (2010) 060; A. Denner, S. Dittmaier, T. Kasprzik, and A. Mück, J. High Energy Phys. 06 (2011) 069, and references therein.

[7] C. Bernaciak and D. Wackeroth, Phys. Rev. D **85**, 093003 (2012), and references therein.

[8] LEPEWWG, TEVEWWG, SLD EW and HF groups, arXiv:1012.2367, and references therein.

[9] G. Altarelli and G. Parisi, Nucl. Phys. **B126**, 298 (1977); Yu. L. Dokshitzer, Sov. Phys. JETP **46**, 641 (1977); L. N. Lipatov, Yad. Fiz. **20**, 181 (1974); V. Gribov and L. Lipatov, Sov. J. Nucl. Phys. **15**, 675 (1972); **15**, 938 (1972); see also J. C. Collins and J. Qiu, Phys. Rev. D **39**, 1398 (1989).

[10] C. G. Callan, Jr., Phys. Rev. D **2**, 1541 (1970); K. Symanzik, Commun. Math. Phys. **18**, 227 (1970); *Springer Tracts in Modern Physics*, edited by G. Hoehler (Springer, Berlin, 1971), Vol. 57, p. 222; see also S. Weinberg, Phys. Rev. D **8**, 3497 (1973).

[11] D. R. Yennie, S. C. Frautschi, and H. Suura, Ann. Phys. (N.Y.) **13**, 379 (1961); see also K. T. Mahanthappa, Phys. Rev. **126**, 329 (1962), for a related analysis.

[12] S. Jadach, B. F. L. Ward, and Z. Wąs, Phys. Rev. D **63**, 113009 (2001).

[13] S. Jadach, B. F. L. Ward, and Z. Wąs, Comput. Phys. Commun. **130**, 260 (2000).

[14] T. K. O. Doan, W. Placzek, and Z. Wąs, arXiv:1303.2220; Report No. CERN-PH-TH-2013-040 (unpublished); Report No. IFJPAN-IV-2013-2 (unpublished).

[15] A. B. Arbusov, R. R. Sadykov, and Z. Wąs, arXiv:1212.6783; Report No. IFJPAN-IV-2012-14 (unpublished); Report No. CERN-PH-TH-2012-354 (unpublished).

[16] S. Jadach, B. F. L. Ward, and Z. Wąs, Eur. Phys. J. C **22**, 423 (2001); Phys. Lett. B **449**, 97 (1999); B. F. L. Ward, S. Jadach, and Z. Wąs, Nucl. Phys. B Proc. Suppl. **116**, 116 (2003), and references therein.

[17] See for example D. M. Kaplan, Report No. FERMILAB-CONF-12-420-APC; A. Conway and H. Wenzel, arXiv:1304.5270; E. Eichten and A. Martin, arXiv:1306.2609, and references therein.

[18] F. Englert and R. Brout, Phys. Rev. Lett. **13**, 321 (1964); P. W. Higgs, Phys. Lett. **12**, 132 (1964); Phys. Rev. Lett. **13**, 508 (1964); G. S. Guralnik, C. R. Hagen, and T. W. B. Kibble, Phys. Rev. Lett. **13**, 585 (1964).

[19] F. Gianotti, in Proc. ICHEP2012 (to be published); G. Aad *et al.*, Phys. Lett. B **716**, 1 (2012).

[20] J. Incandela Proc. Sci., ICHEP2012 (2013) 037; S. Chatrchyan *et al.*, Phys. Lett. B **716**, 30 (2012).

[21] S. Jadach *et al.* (unpublished); V. Halyo *et al.* (unpublished).

[22] See, for example, K. Hamilton and P. Richardson, J. High Energy Phys. 07 (2006) 010.

[23] See, for example, M. Shonherr and F. Krauss, J. High Energy Phys. 12 (2008) 018.

[24] D. Bardin, M. Bilenky, P. Christova, M. Jack, L. Kalinovskaya, A. Olchevski, S. Riemann, and T. Riemann, Comput. Phys. Commun. **133**, 229 (2001).

[25] F. A. Berends, W. L. Van Neerven, and G. J. H. Burgers, Nucl. Phys. **B297**, 429 (1988), and references therein.

[26] S. Jadach, M. Melles, B. F. L. Ward, and S. A. Yost, Phys. Rev. D **65**, 073030 (2002), and references therein.

[27] A. D. Martin, R. G. Roberts, W. J. Stirling, and R. S. Thorne, Eur. Phys. J. C **39**, 155 (2005).

[28] S. Jadach *et al.* (unpublished).

[29] M. Slawinska, S. Jadach, and K. Kutak, Phys. Lett. B **722**, 151 (2013); S. Jadach *et al.*, Proc. Sci., LL2012 (2012) 019; S. Jadach, M. Jeżabek, A. Kusina, W. Płaczek, and M. Skrzypek, Acta Phys. Pol. B **43**, 2067 (2012); K. Kutak, K. Golec-Biernat, S. Jadach, and M. Skrzypek, J. High Energy Phys. 02 (2012) 117; and references therein.

[30] S. Joseph, S. Majhi, B. F. L. Ward, and S. A. Yost, Phys. Lett. B **685**, 283 (2010); S. Joseph, S. Majhi, B. F. L. Ward, and S. A. Yost, Phys. Rev. D **81**, 076008 (2010); B. F. L. Ward, S. Joseph, S. Majhi, and S. A. Yost, Mod. Phys. Lett. A **25**, 2207 (2010); B. F. L. Ward and S. Yost, Proc. Sci., ICHEP2010 (2011) 127; B. F. L. Ward, S. K. Majhi, and S. A. Yost, Proc. Sci., RADCOR2011 (2012) 022; S. K. Majhi, A. Mukhopadhyay, B. F. L. Ward, and S. A. Yost, Phys. Lett. B **719**, 367 (2013); S. K. Majhi *et al.*, arXiv:1305.0023; and references therein.

[31] S. Yost *et al.*, Proc. Sci., RADCOR2011 (2012) 017; and references therein.